Highly Efficient Light-Harvesting Ruthenium Sensitizer for Thin-Film Dye-Sensitized Solar Cells

Chia-Yuan Chen,[†] Mingkui Wang,[‡] Jheng-Ying Li,[†] Nuttapol Pootrakulchote,[‡] Leila Alibabaei,[‡] Cevey-ha Ngoc-le,[‡] Jean-David Decoppet,[‡] Jia-Hung Tsai,[†] Carole Grätzel,[‡] Chun-Guey Wu,[†,*] Shaik M. Zakeeruddin,[‡,*] and Michael Grätzel[‡,*]

[†]Department of Chemistry, National Central University, Jhong-Li, 32001 Taiwan, ROC, and [‡]Laboratory for Photonics and Interfaces, Swiss Federal Institute of Technology, CH 1015 Lausanne, Switzerland

ABSTRACT A high molar extinction coefficient heteroleptic ruthenium complex, incorporating an electron-rich hexylthio-terminal chain, has been synthesized and demonstrated as an efficient sensitizer for dye-sensitized solar cells. With this new sensitizer excellent power conversion efficiency is 11.5% and 4.7% obtained under an irradiation of full sunlight (air mass 1.5 global) in combination with a volatility electrolyte and solid state hole transporting material, respectively. The devices with low volatility electrolyte showed good stability under visible-light soaking at 60 °C during 1000 h of accelerated tests.

KEYWORDS: solar cell · ruthenium · sensitizer · thiophene · impedance spectroscopy · photovoltage transient spectroscopy

During the past two decades, mesoscopic dye-sensitized solar cells (DSCs) have emerged as one of the most promising candidates for practical photovoltaic applications in virtue of their low manufacturing cost and impressive conversion efficiency.[1,2] DSCs demonstrating a conversion efficiency higher than 10% were initially fabricated by using *cis*-di(thiocyanato)-bis-(2,2-bipyridyl)-4,4′-dicarboxylate ruthenium(II) (N3) as the photon-to-current conversion center in combination with a relatively thick titania film and a volatile electrolyte.[3] However, the hydrophilic terminal and light-capturing ability of this sensitizer proved unsatisfactory in permitting DSC devices to achieve robust stability and higher photovoltaic performance. Since this initial time period these drawbacks have been successfully addressed with significant improvement of these criteria through the embodiment of two well-known heteroleptic ruthenium dyes, Z907[4,5] and Z910.[6] Several ruthenium sensitizers have meanwhile been developed using similar strategies.[7−14] Among these dye molecules, a pioneer dye, CYC-B1,[15] exhibiting a remarkably high light-harvesting capacity of up to 2.12 × 10^4 M^{-1} cm^{-1} by incorporating electron-rich thiophene derivatives, has demonstrated the potential of ruthenium dyes with thiophene based ancillary ligands.

Following development of the CYC-B1 dye, several ruthenium dyes were synthesized by incorporating thiophene derivatives into the ancillary ligand. The DSC cells based on these dyes showed excellent photovoltaic performance.[16−21] However, there are only very few ruthenium sensitizers incorporating thiophene derivatives which are capable of exhibiting a metal-to-ligand charge transfer (MLCT) transition's absorption coefficient of more than 2.00 × 10^4 M^{-1} cm^{-1}.[17,22] Thin-film cells based on these highly efficient light-harvesting ruthenium dyes in combination with a low-volatility electrolyte or solid spiro-OMeTAD[23] as a hole-transporting material (HTM) have not thus far been reported. Herein, we report the synthesis of a new heteroleptic ruthenium sensitizer containing hexylthio-bithiophene antennas, coded CYC-B11 (its structure is illustrated in Figure 1) and its application in DSCs. This ruthenium complex with the new concept of thioalkyl substitution shows great promise to become a leading class of robust and panchromatic sensitizers, enabling greatly enhanced DSC performance.

RESULTS AND DISCUSSION

CYC-B11 was synthesized by a typical one-pot reaction as depicted in the experimental section. The electronic absorption spectra of CYC-B11 as well as its anchoring and ancillary ligands measured in DMF are displayed in Figure 2. CYC-B11 shows three absorption bands centered at 305, 388, and 554 nm, respectively. According to the

*Address correspondence to t610002@cc.ncu.edu.tw (C.W.), michael.graetzel@epfl.ch (M.G.), shaik.zakeer@epfl.ch (S.Z.).

Received for review July 7, 2009 and accepted August 31, 2009.

Published online September 11, 2009.
10.1021/nn900756s CCC: $40.75

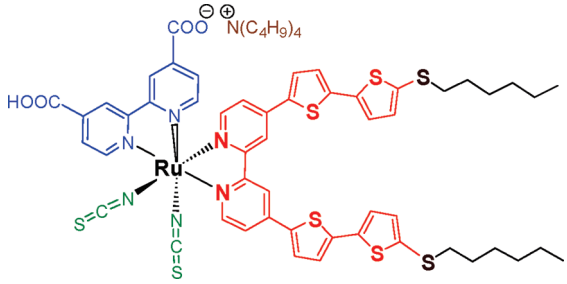

Figure 1. The molecular structure of CYC-B11.

absorption profiles of the free anchoring and ancillary ligands, the band at 305 nm is assigned to the overlap of intraligand $\pi-\pi^*$ transitions of anchoring and ancillary ligands. Another band centered at 388 nm also contains two components: the $\pi-\pi^*$ transition of the ancillary ligand and one of the metal-to-ligand charge transfer (MLCT) transitions for CYC-B11. The molar absorption coefficient ε of the lower energy MLCT band centered at 554 nm is $2.42 \times 10^4\ M^{-1}\ cm^{-1}$, higher than all of the thus reported ruthenium sensitizers incorporating thiophene derivatives for DSCs. This significant augmentation of the MLCT absorption cross section is attributed to the hexylthio-bithiophene antennas' action in increasing both the electron donating ability and extension of the π-conjugation to the bipyridyl ancillary ligand. Moreover, the ε value of CYC-B11 increased by *ca*. 14%, compared to that of its predecessor, CYC-B1[15] (measured in DMF and also displayed in Figure 2). This is primarily because the third row, electron rich sulfur atom has the greater radial orbital extension in its bonding compared to the second row element such as carbon. Inserting a sulfur atom between the thiophene ring and alkyl substituent may result in an increase of the electronic transition dipole momentum and, therefore, the absorption coefficient of the MLCT band.[15] This result reveals that the light-capturing ability of the high molar extinction coefficient ruthenium dyes can be further enhanced by careful design of the electron-donating segments.[24]

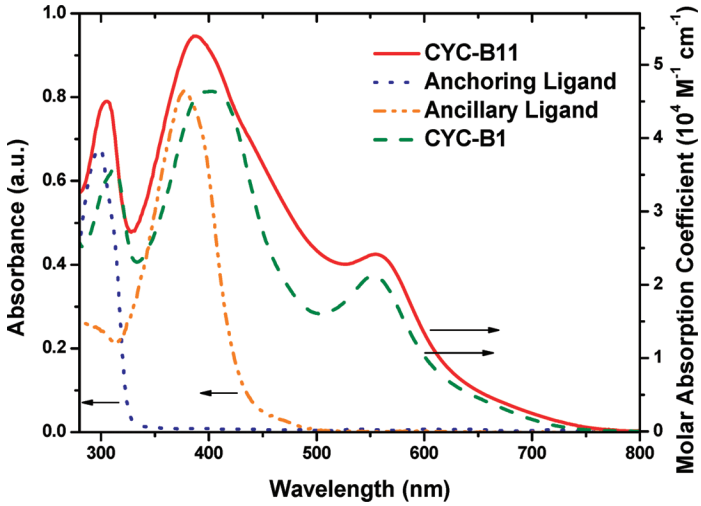

Figure 2. Electronic absorption spectra of CYC-B11, its anchoring and ancillary ligands, and CYC-B1 measured in DMF.

The oxidation potential of CYC-B11, measured by square-wave voltammetry is 0.96 V *versus* NHE (see Figure 3), which is 0.56 V more positive than the redox potential of the iodide/triiodide couple in organic solvents used in a DSC. The optical transition energy, E_{0-0}, of CYC-B11 determined from its absorption onset is 1.58 eV. Neglecting entropy changes during excitation, the excited-state redox potential, ϕ^0 (S^+/S^*) can be determined to be -0.62 V *versus* NHE, which is more negative than the anatase TiO_2 conduction band edge energy level (-0.50 V *versus* NHE). Therefore, upon photoexcitation, CYC-B11 can swiftly inject electrons into the TiO_2 conduction band and then the reduction of oxidized CYC-B11 by the electrolyte will occur spontaneously in this regenerative photovoltaic device.

Some preliminary photovoltaic experiments were conducted to evaluate the performance of the CYC-B11 dye using a volatile acetonitrile-based electrolyte (coded Z960), a low volatile 3-methoxypropionitrile-based electrolyte (coded Z946), and a solid-state organic HTM (coded spiro-OMeTAD), respectively, which were developed by our group.[25] The DSC devices were fabricated and characterized as previously described.[25] Ultrathin and transparent TiO_2 films of only 5 μm thickness were used in initial studies to fabricate photovoltaic devices, rendered possible by the enhanced optical cross section of CYC-B11. The photovoltaic parameters J_{sc}, V_{oc}, FF, and η, of the thin film cell based on CYC-B11 in conjunction with a low-volatility electrolyte (Z946) are 16.1 mA cm^{-2}, 0.714 V, 0.69, and 7.9% (see Table 1), respectively. In the presence of dineohexyl bis-(3,3-dimethyl-butyl)-phosphinic acid (coded DINHOP) as a coadsorbent (4:1 molar ratio in the staining solution), the photovoltaic parameters are 15.5 mA cm^{-2}, 0.732 V, 0.73, and 8.2%. DINHOP has been demonstrated as an effective coadsorbent for reducing the dark current.[26] It is very encouraging to obtain such a high efficiency with a thin transparent titania film (5 μm) using 3-methoxypropionitrile containing low-volatility electrolyte (Z946). These results clearly reveal the advantages of the ruthenium dyes with high molar extinction coefficient. Strikingly, the solid-state dye-sensitized solar cell (SSDSC) device based on CYC-B11 dye using a 2 μm thickness of 20 nm sized TiO_2 transparent film in combination with spiro-OMeTAD as HTM shows a J_{sc} of 9.22 mA cm^{-2}, a V_{oc} of 825 mV and a FF of 0.63 (curve D in Figure 4a) resulting in an impressive efficiency of 4.7% under standard global AM 1.5 solar conditions. At lower light intensity (10 mW cm^{-2}), the power conversion efficiency was 5.3%, which is a high value reported to date for a SSDSC based either on a ruthenium complex or an organic sensitizer.[27−30] The value of J_{sc} for SSDSC devise is lower than that of the liquid device and arises from a lower light-harvesting yield due to the use of thinner TiO_2 film.

These results emphasize the potential capacity of improvement in photovoltaic parameters through the utilization of high molar extinction coefficient ruthenium dyes in the fabrication of SSDSCs. The overall good performance of these devices can be attributed to the formation of a compact interface as well as to a good wetting of the surface with the hole-transport material due to the amphiphilic structure of the dye molecule.

In DSCs, the thickness of the TiO_2 film plays a vital role on the cell performance. By using a 8 μm thick, 20 nm titania transparent film with a second 5 μm thick layer of 400 nm sized light scattering anatase particles, the efficiency of devices with the low-volatility electrolyte (Z946) was further increased to 9.4% (Table 1). At lower light intensity of 50 mW cm^{-2}, the efficiency of the device was as high as 9.8%. Figure 4a (curve B) presents the photocurrent density−voltage characteristic curve of an acetonitrile-based electrolyte (Z960) DSC under standard AM 1.5G simulated sunlight (100 mW cm^{-2}) illumination. The CYC-B11-sensitized cell provides a J_{sc} of 20.05 mA cm^{-2}, a V_{oc} of 0.743 V and a FF of 0.77, yielding an overall power conversion efficiency (η) of 11.5%. The incident photon-to-current conversion efficiency (IPCE) spectrum (as shown Figure 4b) shows a plateau of over 80% from 460 to 685 nm with the maximum of 95% at 580 nm. Considering the light absorption and scattering loss by the conducting glass, the maximum efficiency for absorbed photon-to-collected electron conversion efficiency is close to unity over a broad spectral range. The J_{sc} agrees with the value calculated from the overlap integral of the IPCE spectrum with standard AM 1.5G solar emission spectrum showing that the spectral mismatch of simulated sunlight is less than 2%. To the best of our knowledge this is the highest efficiency published for a volatile electrolyte containing DSC.

A low volatility electrolyte based device was used to evaluate the preliminary stability of the CYC-B11 sensitizer under moderate thermal stress and visible-light soaking. Figure 5 presents the variation in the photovoltaic parameters of CYC-B11 sensitized cells when subjected to the accelerating test in a solar simulator at full sunlight (100 mW cm^{-2}) and 60 °C. Over the entire 1000 h light soaking test period, the photovoltaic parameters J_{sc}, V_{oc}, FF, and η of the cell vary only slightly from the initial values. During the aging process, the value of the efficiency retained 93% of its initial value after 1000 h light soaking, a small drop of 62 mV in V_{oc} being compensated by an increase in the J_{sc} values. Such an impressively stable performance implies the robustness of CYC-B11 dye itself as well as the dye sensitized heterojunction interface.

Unraveling of the details of the electron recombination dynamics between the photoinjected electrons at the TiO_2 and the oxidized

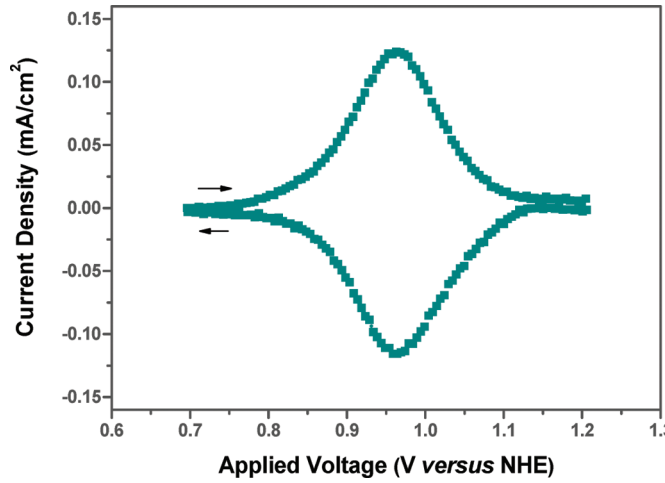

Figure 3. Square-wave voltammogram of CYC-B11 measured in DMF: supporting electrolyte, 0.1 M $TBAPF_6$; potential step increment, 10 mV; frequency, 25 Hz.

TABLE 1. Detailed Photovoltaic Parameters of CYC-B11-Sensitized Devices of Varying Film Thicknesses in the Presence and Absence of DINHOP as Co-adsorbent under Full Sunlight Intensity[a]

device	TiO_2 thickness (μm)	J_{sc} (mA/cm²)	V_{oc} (V)	FF	η (%)
CYC-B11	5	16.1	0.714	0.69	7.9
CYC-B11 + DINHOP (4:1)	5	15.5	0.732	0.73	8.2
CYC-B11	8+5	18.0	0.686	0.68	8.4
CYC-B11 + DINHOP (4:1)	8+5	18.3	0.704	0.73	9.4

[a]The spectral distribution of incident sunlight simulates AM 1.5G solar irradiation. A low-volatility electrolyte (Z946) was used.

electrolyte in various devices was undertaken by employing transient photovoltage measurements, also known as V_{oc} decays. Figure 6a illustrates the extracted charge density *versus* open circuit voltage plot for the fresh and aged liquid and solid-state DSCs. The open-circuit voltage is lower for the aged device at all charge densities examined (*ca.* 74 mV difference at a charge density of 0.94 × 10^{18} cm^{-3}). The solid-state DSC shows the highest V_{oc} contribu-

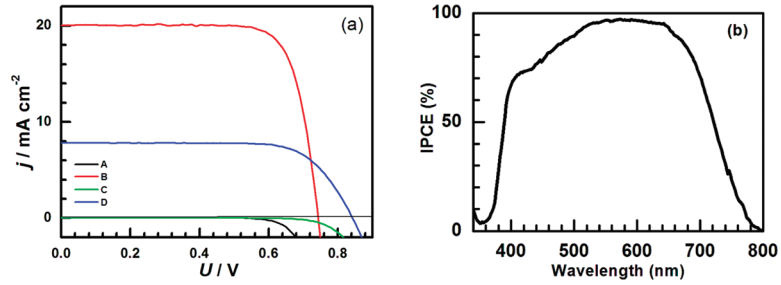

Figure 4. (a) Photocurrent density−voltage characteristic curves of various DSC devices based on CYC-B 11 dye measured in the dark (curves A and C) and under an illumination of the AM 1.5G full sunlight intensity (100 mW cm^{-2}) (curves B and D). Curves A and B are measured with the devices using a volatile electrolyte (Z960) with 8 + 5 μm thick double layer TiO_2 film and a cell active area of 0.158 cm^2 tested with a mask. Curves C and D are measured with the device using solid-state HTM (spiro-OMeTAD) with 2 μm thick TiO_2 film and a cell active area of 0.23 cm^2 tested with a mask. (b) Photon-to-current action spectrum of the liquid device using Z960 electrolyte in panel a.

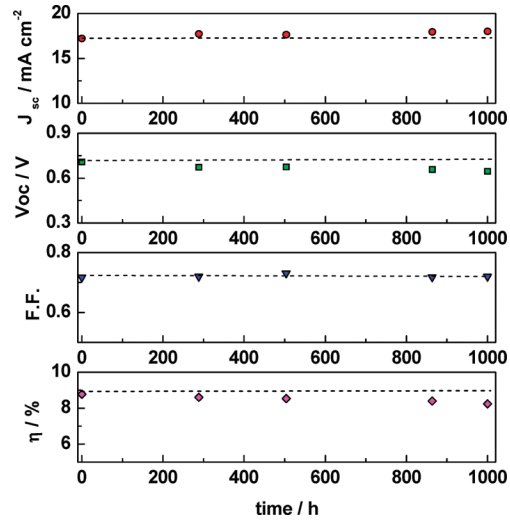

Figure 5. Evolution of the photovoltaic parameters (J_{sc}, V_{oc}, FF, and η) for the device based on (8 + 5) μm TiO_2 double-layer film sensitized with CYC-B11 in the presence of DINHOP (4: 1 molar ratio) as a coadsorbent and low-volatility liquid electrolyte (Z946) during the visible light-soaking (100 mW cm^{-2}) at 60 °C.

tion mainly from a lower hole Fermi level in spiro-OMeTAD, which will be discussed below in more detail. The differences in voltage may be due to (a) a shift on the TiO_2 conduction band with respect to the redox potential of electrolytes or (b) difference in the dye-sensitized heterojunction interfacial recombination reaction. Figure 6b shows the recombination lifetime for various devices. Following the increase of the extracted charge density from the TiO_2 films, the recombination lifetimes (τ_e) become shorter due to the higher electron density at the TiO_2 and larger driving forces for the interfacial recombination. Clearly, the trend of the charge recombination lifetime of the various devices is well in agreement with that of the above measured photocurrent densities. The recombination lifetime in the fresh and aged liquid device exhibits only minor differences, showing an almost complete independence with respect to the time of light soaking. The V_{oc} of the DSC is determined by the potential difference between the quasi-Fermi level of the electrons at the TiO_2 film and the redox potential of the electrolyte. The former is related to the electron steady-state concentration under illumination, which depends on the energy offset between the Fermi level and the conduction band potential.[25] Thus, we conclude that the lower observed V_{oc} of the aged liquid electrolyte-based device (at identical electron densities as those measured in the fresh device) is most likely related to a positive shift (*versus* NHE) of the TiO_2 conduction band potential following light soaking, since the electron lifetimes measured for both fresh and aged cells are very close. The positive shift (*versus* NHE) of conduction band potential may originate from the photoinduced proton intercalation into the titania close to the TiO_2 surface, during the long-term light soaking test.[31−33,13] The recombination lifetime is much shorter in the SSDSC, a main limiting step in obtaining high-efficiency in this kind of device.[25]

Impedance analysis was likewise utilized to monitor the photovoltaic parameter changes in various devices, which is a method scrutinized by our group.[25,26] Figure 6c presents the effect of the applied voltage on the electron transport resistance R_t under dark conditions for the fresh and aged liquid based and solid state DSCs. For comparison, the resistance in the bare TiO_2 (the blank experiments without an adsorbing dye layer on the TiO_2) is also provided. The logarithm of the electron transport resistance, which depends on the number of free electrons ([e^-]) in the conduction band, shows parallel behavior for various devices. This implies that the shift of the resistances for the steady state electron transport in those devices is caused by a change in position of the conduction band edge (E_{cb}).[25,26] In the case of the CYC-B11/DINHOP cografted TiO_2 film (fresh device), a downward shift of the conduction band edge energy level (E_{cb}) by approximately 38 mV with respect to the Fermi level of the redox couple (I^-/I_3^-) was clearly observed compared to the bare TiO_2 within the same electrolyte (Z946 in this case). A similar phenomenon was witnessed for the SSDSC device using spiro-OMeTAD. This displacement arises from the protonation of the titania sur-

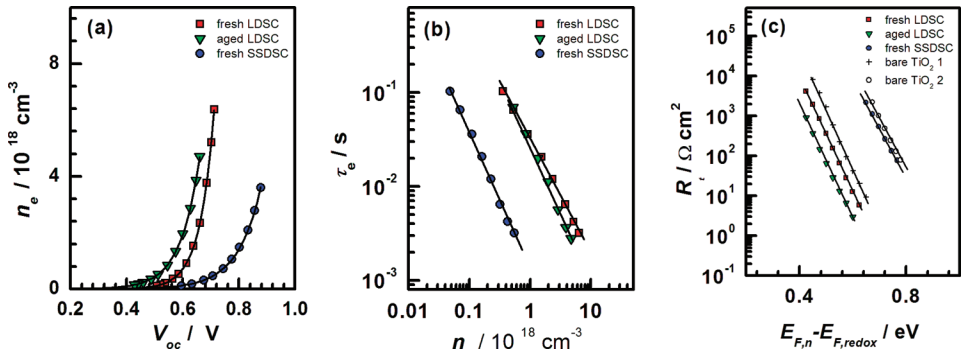

Figure 6. Transient photovoltage decay measurements of the fresh and aged devices with CYC-B11 and DINHOP (4:1 molar ratio): (a, b) effect of light soaking on the relationship (a) between the photoinduced charge density and open circuit voltage and (b) between the recombination lifetime and the photoinduced charge density; (c) electron transport resistance R_t, of the TiO_2 film obtained from impedance measurements in the dark at 20 °C as a function of applied forward bias voltage for the liquid electrolyte based DSC (LDSC) and solid-state DSC (SSDSC) devices. The resistances for the bare TiO_2 (no dye adsorbed) with Z946 (bare TiO_2 1) and spiro-OMeTAD (bare TiO_2 2) were provided for comparison as blank devices. The parameters (n_e and R_t) were normalized with respect to the TiO_2 film thickness, taking into account the porosity (67% for 20 nm TiO_2 transparent layer and 42% for the 400 nm TiO_2 scatting layer from BET measurements) for deriving the content of solid within the nanocrystalline film.

face occurring when dye and coadsorbent molecules are linked onto the oxides by the anchoring groups.[26] Taking into account that there is around 300 mV difference between the redox potential of the electrolyte and the Fermi level of holes in solid-state HTM,[25] it is not surprising to see a large displacement of R_t for the SSDSC with respect to that of liquid devices. A further 49 mV downward shift of E_{cb} (relative to CYC-B11/DINHOP cografted TiO_2 fresh device) was detected for the aged sample. The computed conduction band energy level shift with respect to the Fermi levels of the different HTMs is in very good agreement with the experimental photovoltaic results. This energy shift influences principally the open circuit voltage of the DSC device, an observation that has likewise been confirmed by transient photovoltage decay measurements. Therefore, we anticipate that through stabilizing the TiO_2 conduction band potential by using new coadsorbents, the drop in the open circuit voltage during the aging process can be significantly controlled.

SUMMARY

We have reported a new heteroleptic ruthenium sensitizer, CYC-B11, incorporating electron-rich hexylthio-bithiophene antennas. This new dye exhibits an excellent light-harvesting capacity, greater than all of the heretofore-reported ruthenium dyes incorporating thiophene derivatives for DSCs. The corresponding DSC cell using a volatile liquid electrolyte exhibits an excellent conversion efficiency of 11.5% under AM 1.5G simulated sunlight. The cell employing a low-volatility electrolyte shows good performance and stability under prolonged light soaking at 60 °C. Furthermore, the solid-state DSC based on CYC-B11 with spiro-OMeTAD as a hole transport material displays an impressive efficiency of 4.7% under AM 1.5G simulated sunlight. These initial results clearly demonstrate the benefits for improvements in performance and stability through the use of highly proficient light-harvesting ruthenium dyes in the thin film DSC. These types of cells are very promising and higher photovoltaic efficiencies will most certainly be obtained in the future. The cell optimization, as well as the studies of the CYC-B11-sensitized cells using solvent-free ionic liquid electrolyte in the thin film DSC systems, is currently underway in order to fully explore the prospective of this promising dye molecule.

METHODS

Materials. All reagents were obtained from commercial sources and used as received except when specified. Solvents were dried over sodium or CaH_2 before use. The DINHOP coadsorbent was synthesized as reported in an earlier publication.[26] The structures of CYC-B11 dye and its intermediates were identified by ^{1}H NMR spectra. The structure of CYC-B11 dye was further confirmed by FAB-MS analysis and elemental analysis.

Synthesis of CYC-B11. This new ruthenium dye was synthesized by a typical one-pot reaction using ligand-11, which is prepared as follows.

Preparation of 2-(Hexylthio)thiophene. Thiophene (10.0 g (0.119 mol)) was dissolved in 45.0 mL of anhydrous ether; this solution was cooled to −78 °C, and a total of 47.0 mL (0.118 mol) of *n*-BuLi (2.5 M in hexane) was then added dropwise into the solution that was kept under continuous stirring for 1.5 h at −78 °C. A quantity of 3.80 g of sulfur powder (0.118 mol) was added in one portion into the reaction mixture, and the mixture was stirred continuously at −78 °C for 2 h. 1-Bromohexane (19.4 g (0.118 mol)) was added dropwise to the mixture that was stirred continuously overnight at room temperature. The addition of crushed ice containing NH_4Cl terminated the reaction. Following the formation of the heterogeneous solution, the organic layer was collected and the aqueous layer was further extracted with ether. Two organic portions were combined and the impurities were extracted with saturated $NaHCO_{3(aq)}$, distilled water, and saturated $NaCl_{(aq)}$, respectively. The crude product was further purified by chromatography using hexane as an eluent to afford 16.5 g (69.6% yield) of the product. ^{1}H NMR (300 MHz, $CDCl_3$), δ (ppm): 7.32 (dd, 1H), 7.10 (dd, 1H), 6.97 (dd, 1H), 2.79 (t, 2H), 1.59 (m, 2H), 1.41 (m, 2H), 1.28 (m, 4H), 0.90 (t, 3H). MS calcd: *m/z* 200.07 ($[M]^+$). LRFAB-MS found: *m/z* 200.1 (m) ($[M]^+$).

Preparation of 5-(Hexylthio)-2,2′-bithiophene. The 5-(hexylthio)-2,2′-bithiophene was prepared by Stille coupling of trimethyl (5-hexylthio-2,2′-bithiophen-5′-yl) stannane and 2-bromothio-phene using the procedures similar to those reported previously.[15] Trimethyl(5-hexylthio-2,2′-bithiophen-5′-yl) stannane was prepared by adding 13.0 mL (32.5 mmol) of *n*-BuLi (2.5 M in hexane) into a solution of 6.50 g (32.4 mmol) of 2-(hexylthio)thiophene dissolved in 40.0 mL of anhydrous THF at −78 °C and followed by adding 6.50 g (32.6 mmol) of trimethyltin chloride dissolved in anhydrous THF at −78 °C. The mixture was stirred overnight at room temperature, and the reaction was terminated by adding saturated $NaCl_{(aq)}$. The crude product was extracted with CH_2Cl_2. After the solvent was removed, 10.7 g (90.9% yield) of crude product, trimethyl(5-hexylthio-2,2′-bithiophen-5′-yl) stannane, was obtained. This material was used without further purification in the following procedure. A 10.7 g (29.5 mmol) portion of crude trimethyl(5-hexylthio-2,2′-bithiophen-5′-yl) stannane and 4.80 g (29.5 mmol) of 2-bromothiophene were dissolved in 50 mL of anhydrous DMF with 2.05 g (1.77 mmol) of $Pd(PPh_3)_4$ added as a catalyst. The mixture was refluxed under argon for 48 h. After the mixture was cooled to room temperature, 5 wt % $NH_4Cl_{(aq)}$ was added to terminate the reaction and the mixture was extracted with CH_2Cl_2. The organic layer was collected and the impurities were then extracted by using saturated $NaHCO_{3(aq)}$, distilled water, and saturated $NaCl_{(aq)}$, respectively. The crude product was further purified by chromatography using hexane as an eluent to afford 6.01 g (72% yield) of the product. ^{1}H NMR (300 MHz, $CDCl_3$), δ (ppm): 7.21 (dd, 1H), 7.14 (dd, 1H), 7.01 (m, 3H), 2.81 (t, 2H), 1.64 (m, 2H), 1.44 (m, 2H), 1.38 (m, 4H), 0.90 (t, 3H). MS calcd: *m/z* 282.06 ($[M]^+$). LRFAB-MS found: *m/z* 282.05 (m) ($[M]^+$).

Synthesis of Ligand-11 (4,4′-Bis(5-(hexylthio)-2,2′-bithien-5′-yl)-2,2′-bipyridine). Ligand-11 was prepared by Stille coupling of trimethyl-(5′-(5-(hexylthio)-2,2′-bithiophene) stannane and 4,4′-dibromo-2,2′-bipyridine prepared according to procedures similar to the preparation of 5-(hexylthio)-2,2′- bithiophene reported previously.[15] A 3.29 g (7.38 mmol) portion of trimethyl-(5′- (5-(hexylthio)-2,2′-bithiophene) stannane crude product and 1.00 g (3.18 mmol) of 4,4′-dibromo-2,2′-bipyridine were dissolved in 50 mL anhydrous DMF, to which 0.51 g (0.44 mmol) of $Pd(PPh_3)_4$ was added as a catalyst. The mixture was refluxed under argon for 48 h. After the mixture was cooled to room temperature, 5 wt % NH_4Cl(aq) was added to terminate the reaction, and the product was extracted with $CHCl_3$. The organic layer was washed

with saturated $NaHCO_{3(aq)}$, distilled water, and saturated $NaCl_{(aq)}$. The crude product (Ligand-11) was purified by recrystallization from hexane (66.0% yield). ^{1}H NMR (300 MHz, $CDCl_3$), δ (ppm): 8.66 (d, 4H), 7.56 (d, 2H), 7.48 (d, 2H), 7.17 (d, 2H), 7.10 (d, 2H), 7.02 (d, 2H), 2.83 (t, 4H), 1.43 (m, 4H), 1.27 (m, 12H), 0.88 (t, 6H). MS calcd: *m/z* 716.15 ($[M]^+$). LRFAB-MS found: *m/z* 717.5 (m) ($[M+H]^+$).

CYC-B11 (TBA(Ru[(4-carboxylic acid-4′-carboxylate-2,2′-bipyridine)(Ligand-11)(NCS)$_2$])). CYC-B11 was synthesized using the one-pot synthetic procedure similar to the reaction protocol we had reported previously:[15] 0.202 g (0.330 mmol) of $[RuCl_2(p\text{-cymene})]_2$, 0.473 g (0.660 mmol) of Ligand-11, 0.161 g of (0.660 mmol) dcbpy (4,4′-dicarboxylic acid-2,2′- bipyridine), and excess NH_4NCS were used in the reaction. The crude product was dissolved in a mixture of methanol and tetra-butyl ammonium hydroxide (TBAOH) aqueous solution (40 wt % in H_2O) and then purified on a Sephadex LH-20 column, using methanol as an eluent. The main band was collected and the pH value of the collected solution was lowered to *ca.* 5.7 by adding dilute HNO_3. The collected precipitate was washed with water and dried under vacuum. After purification, 0.330 g (0.232 mmol, 35.2% yield) of CYC-B11 was obtained. ^{1}H NMR (500 MHz, DMSO-d_6), δ (ppm): 9.36 (d, J = 5.4 Hz, 1H); 9.20 (d, J = 6.0 Hz, 1H); 9.10 (s, 1H); 9.05 (s, 1H); 8.94 (s, 1H); 8.89 (s, 1H); 8.27 (d, J = 3.5 Hz, 2H); 8.21 (d, J = 5.6 Hz, 1H); 8.04 (d, J = 3.9 Hz, 1H); 7.84 (d, J = 5.4 Hz, 1H); 7.61 (d, J = 3.8 Hz, 1H); 7.59 (d, J = 5.6 Hz, 1H); 7.48 (d, J = 3.8 Hz, 1H); 7.46 (d, J = 3.6 Hz, 1H); 7.44 (d, J = 6.0 Hz, 1H); 7.39 (d, J = 5.6 Hz, 1H); 7.35 (d, J = 3.6 Hz, 1H); 7.21 (d, J = 3.7 Hz, 1H); 7.14 (d, J = 3.7 Hz, 1H); 3.16 (t, 8H); 2.83 (t, 2H); 2.78 (t, 2H); 1.56 (m, 12H); 1.27 (m, 20H); 0.93 (t, 12H); 0.85 (m, 6H). MS calcd: *m/z* 1419.33 ($[M]^+$); 1177.05 ($[M-N(C_4H_9)_4]^+$). LRFAB-MS found: *m/z* 1178.2 (m) ($[M+H-N-(C_4H_9)_4]^+$); 1120.2 (s) ($[M+H-N(C_4H_9)_4\text{-}NCS]^+$). HRFAB-MS found: 1178.0551, ($[M+H-N(C_4H_9)_4]^+$). Anal. Calcd for $C_{68}H_{83}N_7O_4RuS_8 \cdot 2H_2O$: C, 56.09; H, 6.02; N, 6.73; S, 17.62%. Found: C, 55.91; H, 5.47; N, 6.77; S, 17.41%.

Device Fabrication. The cells consisted of a mesoscopic TiO_2 film composed of a 8-μm thick transparent layer of 20 nm sized TiO_2 anatase nanoparticles onto which a second 5 μm thick scattering layer of 400 nm sized TiO_2 was superimposed. The double layer films were heated to 520 °C and sintered for 30 min, then cooled to 80 °C and immersed into the dye solution (300 μM) containing 10 % DMSO in acetonitrile and *tert*-butyl alcohol (volume ratio: 1:1) mixture with 75 μM DINHOP as a coadsorbent for 16 h. In the liquid-state devices, either a volatile or a low-volatility electrolyte coded Z960 or Z946, respectively, was used. The Z960 electrolyte contains 1.0 M 1,3-dimethylimidazolium iodide (DMII), 50 mM LiI, 30 mM I_2, 0.5 M *ter*-butylpyridine, and 0.1 M guanidinium thiocyanate (GNCS) in the mixed solvent of acetonitrile and valeronitrile (v/v, 85/15). The Z946 electrolyte contains 3-methoxypropionitrile as a solvent and 1.0 M DMII, 0.15 M I_2, 0.5 M NBB as well as 0.1 M GNCS as solutes. The cell was sealed with a 25 μm-thick transparent Surlyn ring (from DuPont) at 130 °C for 15 s to the counter-electrode (FTO glass, 15 Ω per square, coated with a platinum solution chemically deposited at 450 °C for 15 min). The cells were filled with an electrolyte solution through a predilled hole in the counter-electrode. The hole was then sealed with a Bynel disk and a thin glass to avoid leakage of the electrolyte. For the solid-state devices, a compact TiO_2 layer was first deposited onto the FTO substrate by spray pyrolysis, onto which 20 nm sized TiO_2 particles were deposited by doctor-blading to obtain a 2 μm thick mesoporous film. After sintering the TiO_2 layers at 500 °C, the film was cooled to room temperature and immersed overnight in 0.02 M aqueous $TiCl_4$. The film was then rinsed with deionized water, annealed in air at 450 °C for 20 min, and cooled to 80 °C before immersing it in the above-mentioned dye solution for sensitization. The hole conductor matrix was applied by spin-coating of a spiro-OMeTAD solution. The spiro-OMeTAD solution (137 mM in chlorobenzene) contains final concentrations of 112 mM *tert*-butylpyridine and 21 mM $Li[CF_3SO_2]_2N$ (added from highly concentrated acetonitrile solutions). Finally, a gold contact (100 nm) was deposited on the organic semiconductor film by evaporation (EDWARDS AUTO 500 Magnetron Sputtering System).

Physicochemical and Photovoltaic Performance Measurements. ^{1}H NMR spectra were recorded with Bruker 200 or 500 MHz NMR spectrometer in $CDCl_3$ or DMSO-d_6. FAB-MS spectra were obtained using JMS-700 HRMS. UV/vis spectra were measured using a Cary 300 Bio spectrometer. Voltammetric measurements were performed in a single-compartment, three-electrode cell with a platinum disk working electrode and a Pt wire counter-electrode. The reference electrode was Ag/Ag^+ and the supporting electrolyte was 0.1 M $TBAPF_6$ (tetrabutylammonium hexafluorophosphate) in DMF. The square-wave voltammogram was recorded using an Autolab system (PGSTAT 30, Autolab, Eco-Chemie, The Netherlands), and the ferrocene/ferrocinium redox couple was used as a calibration standard. Elemental analyses were carried out with a Heraeus CHN-O-S Rapid-F002 analysis system. The photovoltaic performance, transient photoelectrical, and electrochemical impedance spectroscopy (EIS) of the DSC devices were measured using set-ups similar to those reported in the literature.[25]

Device Stability Test. The cell was covered with a 50 μm thick polyester film acting as a UV cutoff filter for the accelerated testing. The test was performed under illumination with visible light (1 sun; 100 mW/cm^2) at 60 °C, and the photovoltaic performance during the test was recorded. The physicochemical measurements were conducted at room temperature after the cell was equilibrated and cooled down to room temperature.

Acknowledgment. The financial support from the National Science Council, Taiwan, ROC and the Swiss National Science Foundation was gratefully acknowledged.

REFERENCES AND NOTES

1. O'Regan, B.; Grätzel, M. A Low-Cost, High-Efficiency Solar Cell Based on Dye-Sensitized Colloid TiO_2 Films. *Nature* **1991**, *353*, 737–740.
2. Grätzel, M. Photoelectrochemical Cells. *Nature* **2001**, *414*, 338–344.
3. Nazeeruddin, M. K.; Kay, A.; Rodicio, L.; Humpbry-Baker, R.; Miiller, E.; Liska, P.; Vlachopoulos, N.; Grätzel, M. Conversion of Light to Electricity by *cis*-X_2Bis(2,2′-bipyridyl-4,4′-dicarboxylate)ruthenium(II) Charge-Transfer Sensitizers (X = C1$^-$, Br$^-$, I$^-$, CN$^-$, and SCN$^-$) on Nanocrystalline TiO_2 Electrodes. *J. Am. Chem. Soc.* **1993**, *115*, 6382–6390.
4. Zakeeruddin, S. M.; Nazeeruddin, M. K.; Humphry-Baker, R.; Péchy, P.; Quagliotto, P.; Barolo, C.; Viscard, G.; Grätzel, M. Design, Synthesis, and Application of Amphiphilic Ruthenium Polypyridyl Photosensitizers in Solar Cells Based on Nanocrystalline TiO_2 Films. *Langmuir* **2002**, *18*, 952–954.
5. Wang, P.; Zakeeruddin, S. M.; Moser, J. E.; Nazeeruddin, M. K.; Sekiguchi, T.; Grätzel, M. A Stable Quasi-Solid-State Dye-Sensitized Solar Cell with an Amphiphilic Ruthenium Sensitizer and Polymer Gel Electrolyte. *Nat. Mater.* **2003**, *2*, 402–407.
6. Wang, P.; Zakeeruddin, S. M.; Moser, J. E.; Humphry-Baker, R.; Comte, P.; Aranyos, V.; Hagfeldt, A.; Nazeeruddin, M. K.; Grätzel, M. Stable New Sensitizer with Improved Light Harvesting for Nanocrystalline Dye-Sensitized Solar Cells. *Adv. Mater.* **2004**, *16*, 1806–1811.
7. Wang, P.; Klein, C.; Humphry-Baker, R.; Zakeeruddin, S. M.; Grätzel, M. A High Molar Extinction Coefficient Sensitizer for Stable Dye-Sensitized Solar Cells. *J. Am. Chem. Soc.* **2005**, *127*, 808–809.
8. Jiang, K. J.; Masaki, N.; Xia, J. B.; Noda, S.; Yanagida, S. A Novel Ruthenium Sensitizer with a Hydrophobic 2-Thiophen-2-yl-vinyl-Conjugated Bipyridyl Ligand for Effective Dye Sensitized TiO_2 Solar Cells. *Chem. Commun.* **2006**, 2460–2462.
9. Jang, S. R.; Lee, C.; Choi, H.; Ko, J.; Lee, J.; Vittal, R.; Kim, K. J. Oligophenylenevinylene-Functionalized Ru(II)-bipyridine Sensitizers for Efficient Dye-Sensitized Nanocrystalline TiO_2 Solar Cells. *Chem. Mater.* **2006**, *18*, 5604–5608.

10. Chen, C. Y.; Lu, H. C.; Wu, C. G.; Chen, J. G.; Ho, K. C. New Ruthenium Complexes Containing Oligoalkylthiophene-Substituted 1,10-Phenanthroline for Nanocrystalline Dye-Sensitized Solar Cells. *Adv. Funct. Mater.* **2007**, *17*, 29–36.
11. Kuang, D.; Klein, C.; Ito, S.; Moser, J. E.; Humphry-Baker, R.; Evans, N.; Duriaux, F.; Grätzel, C.; Zakeeruddin, S. M.; Grätzel, M. High-Efficiency and Stable Mesoscopic Dye-Sensitized Solar Cells Based on a High Molar Extinction Coefficient Ruthenium Sensitizer and Nonvolatile Electrolyte. *Adv. Mater.* **2007**, *19*, 1133–1137.
12. Lee, C.; Yum, J. H.; Choi, H.; Kang, S. O.; Ko, J.; Humphry-Baker, R.; Grätzel, M.; Nazeeruddin, M. K. Phenomenally High Molar Extinction Coefficient Sensitizer with "Donor-Acceptor" Ligands for Dye-Sensitized Solar Cell Applications. *Inorg. Chem.* **2008**, *47*, 2267–2273.
13. Matar, F.; Ghaddar, T. H.; Walley, K.; DosSantos, T.; Durrant, J. R.; O'Regan, B. A New Ruthenium Polypyridyl Dye, TG6, Whose Performance in Dye-Sensitized Solar Cells is Surprisingly Close to That of N719, the 'Dye to Beat' for 17 Years. *J. Mater. Chem.* **2008**, *18*, 4246–4253.
14. Jang, S. R.; Yum, J. H.; Klein, C.; Kim, K. J.; Wagner, P.; Officer, D.; Grätzel, M.; Nazeeruddin, M. K. High Molar Extinction Coefficient Ruthenium Sensitizers for Thin Film Dye-Sensitized Solar Cells. *J. Phys. Chem. C* **2009**, *113*, 1998–2003.
15. Chen, C. Y.; Wu, S. J.; Wu, C. G.; Chen, J. G.; Ho, K. C. A Ruthenium Complex with Superhigh Light-Harvesting Capacity for Dye-Sensitized Solar Cells. *Angew. Chem.* **2006**, *118*, 59545957;. *Angew. Chem. Int. Ed.* **2006**, *45*, 5822−5825.
16. Chen, C. Y.; Wu, S. J.; Li, J. Y.; Wu, C. G.; Chen, J. G.; Ho, K. C. A New Route to Enhance the Light-Harvesting Capability of Ruthenium Complexes for Dye-Sensitized Solar Cells. *Adv. Mater.* **2007**, *19*, 3888–3891.
17. Gao, F.; Wang, Y.; Zhang, J.; Shi, D.; Wang, M.; Humphry-Baker, R.; Wang, P.; Zakeeruddin, S. M.; Grätzel, M. A New Heteroleptic Ruthenium Sensitizer Enhances the Absorptivity of Mesoporous Titania Film for a High Efficiency Dye-Sensitized Solar Cell. *Chem. Commun.* **2008**, 2635–2637.
18. Gao, F.; Wang, Y.; Shi, D.; Zhang, J.; Wang, M.; Jing, X.; Humphry-Baker, R.; Wang, P.; Zakeeruddin, S. M.; Grätzel, M. Enhance the Optical Absorptivity of Nanocrystalline TiO_2 Film with High Molar Extinction Coefficient Ruthenium Sensitizers for High Performance Dye-Sensitized Solar Cells. *J. Am. Chem. Soc.* **2008**, *130*, 10720–10728.
19. Shi, D.; Pootrakulchote, N.; Li, R.; Guo, J.; Wang, Y.; Zakeeruddin, S. M.; Grätzel, M.; Wang, P. New Efficiency Records for Stable Dye-Sensitized Solar Cells with Low-Volatility and Ionic Liquid Electrolytes. *J. Phys. Chem. C* **2008**, *112*, 17046–17050.
20. Chen, C. Y.; Chen, J. G.; Wu, S. J.; Li, J. Y.; Wu, C. G.; Ho, K. C. Multifunctionalized Ruthenium-Based Supersensitizers for Highly Efficient Dye-Sensitized Solar Cells. *Angew. Chem.* **2008**, *120*, 7452–7455; *Angew. Chem. Int. Ed.* **2008**, *47*, 7342−7345.
21. Abbotto, A.; Barolo, C.; Bellotto, L.; De Angelis, F.; Grätzel, M.; Manfredi, N.; Marinzi, C.; Fantacci, S.; Yum, J. H.; Nazeeruddin, M. K. Electron-Rich Heteroaromatic Conjugated Bipyridine Based Ruthenium Sensitizer for Efficient Dye-Sensitized Solar Cells. *Chem. Commun.* **2008**, 5318–5320.
22. Choi, H.; Baik, C.; Kim, S.; Kang, M. S.; Xu, X.; Kang, H. S.; Kang, S. O.; Ko, J.; Nazeeruddin, M. K.; Grätzel, M. Molecular Engineering of Hybrid Sensitizers Incorporating an Organic Antenna into Ruthenium Complex and Their Application in Solar Cells. *New J. Chem.* **2008**, *32*, 2233–2237.
23. Bath, U.; Lupo, D.; Comte, P.; Moser, J. E.; Weissörtel, F.; Salbeck, J.; Spreitzer, H.; Grätzel, M. Solid-State Dye-Sensitized Mesoporous TiO_2 Solar Cells with High Photon-to-Electron Conversion Efficiencies. *Nature* **1998**, *395*, 583–585.
24. While preparing this manuscript we discovered a publication employing a similar concept by using alkylthio substituent on the bipyridine to increase the molar extinction coefficient of ruthenium sensitizers. Cao, Y.; Bai, Y.; Yu, Q.; Cheng, Y.; Liu, S.; Shi, D.; Gao, F.; Wang, P. Dye-Sensitized Solar Cells with a High Absorptivity Ruthenium Sensitizer Featuring a 2-(Hexylthio)thiophene Conjugated Bipyridine. *J. Phys. Chem. C* **2009**, *113*, 6290–6297.
25. Wang, M.; Chen, P.; Humphry-Baker, R.; Zakeeruddin, S. M.; Grätzel, M. The Influence of Charge Transport and Recombination on the Performance of Dye-Sensitized Solar Cells. *ChemPhysChem* **2009**, *10*, 290–299.
26. Wang, M.; Li, X.; Lin, H.; Pechy, P.; Zakeeruddin, S. M.; Grätzel, M. Passivation of Nanocrystalline TiO_2 Junctions by Surface Adsorbed Phosphinate Amphiphiles Enhances the Photovoltaic Performance of Dye Sensitized Solar Cells. Dalton Trans. 2009, DOI: 10.1039/b908673k.
27. Wang, M.; Xu, M.; Shi, D.; Li, R.; Gao, F.; Zhang, G.; Yi, Z.; Humphry-Baker, R.; Wang, P.; Zakeeruddin, S. M.; Graetzel, M. High-Performance Liquid and Solid Dye-Sensitized Solar Cells Based on a Novel Metal-Free Organic Sensitizer. *Adv. Mater.* **2008**, *20*, 4460–4463.
28. Wang, M.; Grätzel, C.; Moon, S.; Humphry-Baker, R.; Rossier-Iten, N.; Zakeeruddin, S. M.; Grätzel, M. Surface Design in Solid-State Dye Sensitized Solar Cells: Effects of Zwitterionic Co-adsorbents on Photovoltaic Performance. *Adv. Func. Mater.* **2009**, *19*, 2163–2172.
29. Schmidt-Mende, L.; Zakeeruddin, S. M.; Grätzel, M. Efficiency Improvement in Solid-State-Dye-Sensitized Photovoltaics with an Amphiphilic Ruthenium-Dye. *Appl. Phys. Lett.* **2005**, *86*, 013504.
30. Snaith, H. J.; Moule, A. J.; Klein, C.; Meerholz, K.; Friend, R. H.; Grätzel, M. Efficiency Enhancements in Solid-State Hybrid Solar Cells *via* Reduced Charge Recombination and Increased Light Capture. *Nano Lett.* **2007**, *7*, 3372–3376.
31. Gerischer, H. Neglected Problems in the pH Dependence of the Flatband Potential of Semiconducting Oxides and Semiconductors Covered with Oxide Layers. *Electrochim. Acta* **1989**, *34*, 1005–1009.
32. Nazeeruddin, M. K.; Humphry-Baker, R.; Liska, P.; Grätzel, M. Investigation of Sensitizer Adsorption and the Influence of Protons on Current and Voltage of a Dye-Sensitized Nanocrystalline TiO_2 Solar Cell. *J. Phys. Chem. B* **2003**, *107*, 8981–8987.
33. Nazeeruddin, M. K.; De Angelis, F.; Fantacci, S.; Selloni, A.; Viscardi, G.; Liska, P.; Ito, S.; Takeru, B.; Grätzel, M. Combined Experimental and DFT-TDDFT Computational Study of Photoelectrochemical Cell Ruthenium Sensitizers. *J. Am. Chem. Soc.* **2005**, *127*, 16835–16847.